WARP-10: A NUMERICAL SIMULATION MODEL FOR THE CYLINDRICAL RECONNECTION LAUNCHER*

SAND--89-2070C

DE90 007287

Melvin M. Widner
Electromagnetic Launcher Division 1221
Sandia National Laboratories
Albuquerque, New Mexico 87185

ABSTRACT

A fully self-consistent computer simulation code called WARP-10, used for modelling the Reconnection Launcher, is described. WARP-10 has been compared with various experiments with good agreement for performance and heating. Simulations predict that it is possible to obtain nearly uniform acceleration with high efficiency and low armature heating. There does not appear to be an armature heating limit to velocity provided the armature mass can be sufficiently large. Simulation results are presented which show it is possible to obtain conditions needed for Earth-to-Orbit (ETO) launch applications (4.15 km/s and a 850 kg launch mass). This 3100-stage launcher has an efficiency of 47.2% and a final ohmic energy/kinetic energy = .00146. The mode of launcher operation is similar to a traveling wave induction launcher and is produced by properly timed and tuned discrete stages. Further optimization and much higher velocities appear possible.

INTRODUCTION

Contactless coil launchers are being developed at Sandia for the purpose of application to Earth-to-Orbit (ETO) missions [1]. The Sandia program grew from early work on the Pulsar system [2] in 1974, the Theta Gun program reported in 1982 [3], and the Reconnection Gun Program [4]. The recent effort employs cylindrical geometry and has added features that control armature heating and produce high efficiency with nearly uniform acceleration. The final velocity is thus not limited by armature heating, and a practical, efficient system can be realized with non-cryogenic coil technology. The approach under study does not require electrical contact with the stator and does not have arcs produced in the barrel. Consequently, to understand the launcher and to predict performance requires only that the coil and armature geometry be known in detail as well as material properties. If the system can be adequately represented, then performance can be predicted from first principles with no adjustable parameters.

*This work supported by the U.S. Department of Energy under Contract No. DE-AC04-76DP00789.

The circuit approach employed in WARP-10 is similar to previous models for induction launchers [3,5]. Early versions of WARP-10 were applied to the plate projectile Reconnection Launcher [4] that was three-dimensional in nature. The cylindrical coil system presently under study is much easier to model and assumes two-dimensional, axisymmetric geometry. The procedures used in WARP-10 could be generalized to 3-D if there were significant departures from axisymmetry, although this does appear necessary for problems and issues under study at this time. In addition to the method of inductance computation, there are many features that are different from previous models such as variable, non-uniform zoning, multiple materials, skin corrections to circuit resistance, coil geometry options, and firing control. Fast code turnaround and automated control of launcher parameters facilitated the development of the present operational method for heating control and high performance.

MODEL

WARP-10 is a fully self-consistent circuit model that is used for modelling the cylindrical induction launchers. The present code model employs 2-D cylindrical geometry with axisymmetry, although earlier versions considered 3-D geometry appropriate for plate projectiles. Multiple, discrete, coupled stages are modeled with each stage a multi-turn, layered coil if so desired. The armature is solid metal with multiple materials and voids possible. Material properties have temperature-dependent resistivity and specific heat. Computation of force distribution and skin effects are also performed. WARP-10 runs on either a VAX or a Cray computer and has a restart capability for running long calculations such as a full scale ETO launcher. Energy conservation is monitored and satisfied to better than one part in 1000.

The simulation model has been validated by numerous experiments and launcher tests. Bench measurements of coil inductance, inductance gradient vs projectile position, coil resistance, B fields at select positions, induced armature currents, and armature heating have been performed with general good agreement. Comparisons with earlier flat plate launcher experiments have also been performed with good agreement for launcher velocity and ablation onset. These experiments obtained final velocities greater than 1 km/s. More recent comparisons with cylindrical experiments have been done at a very small size with a 10 gm armature [6] and at a larger 5 kg size [7].

The launcher is approximated as a lumped circuit model and is illustrated in Fig. 1. A single stage is shown with the projectile. A capacitive energy store is discharged through a closing switch S_1 into the stator coil L_c. The mutual coupling with the armature results in an induced current and a force consistent with the mutual inductance gradient. The armature is subdivided into many circuits and will be discussed later, but is shown here as a single circuit for illustration purposes only. Also shown in the pulse forming network are feed resistances R_a, R_b, and R_d; feed inductances L_a, L_b, and L_d; a shunt diode to limit voltage reversal on the capacitor; a shunt dump resistor included in R_b to reduce action, charge, and current through the switch, diode and the coil; and a coil resistor R_c that has skin and proximity effects [8] included. Mutual coupling between stages is also incorporated in the model but is not shown.

Figure 1. Circuit diagram for a single launcher stage.

The circuit equations used in WARP-10 are standard voltage loop equations derived from flux conservation. For the conditions when the diode circuit is open, WARP-10 solves Eq. 1.

$$(R_a + R_d)I_2 + (L_a + L_d)\frac{dI_2}{dt} + V_c = V \qquad (1)$$

where I_2 = loop current, V_c = coil voltage across R_c and L_c in Figure 1 (Eq. 4), and V = capacitor voltage (Eq. 6). For the case where the diode is closed, WARP-10 solves Eqs. 2 and 3.

$$(R_a + R_b)I_1 + (L_a + L_b)\frac{dI_1}{dt} - R_bI_2 - L_b\frac{dI_2}{dt} = V \qquad (2)$$

$$-R_bI_1 - L_b\frac{dI_1}{dt} + (R_b + R_d)I_2 + (L_b + L_d)\frac{dI_2}{dt} = -V_c \qquad (3)$$

where I_1 is the loop current for the left loop and I_2 the right loop current. The coil voltage is given as

$$R_c I_2 + L_c \frac{dI_2}{dt} + \sum_{\substack{i=1 \\ i \neq k}}^{N_s} M_{ki} \frac{dI_i}{dt} + \sum_{j=1}^{N_p} \frac{d}{dt} M_{kj} I_j = V_c \qquad (4)$$

where M = mutual inductance, I_i = coil current for stage i, i = stage index from 1 to N_s, and j = projectile circuit index from 1 to N_p. Note that Eqs. 1-4 are written for a single reference stage k and that the subscript k has been omitted except in Eq. 4. The loop equation for projectile circuit j is given as

$$R_j I_j + L_j \frac{dI_j}{dt} + \sum_{k=1}^{N_s} \frac{d}{dt} M_{kj} I_k + \sum_{\substack{m=1 \\ m \neq j}}^{N_p} M_{mj} \frac{d}{dt} I_m = 0 \qquad (5)$$

where m is a summation index over projectile circuits. The capacitor voltage is given as

$$V = \begin{cases} 0 & t < t_1 \\ V_o - \frac{1}{C} \int_{t_1}^{t} I_1 dt' & t \geq t_1 \end{cases} \qquad (6)$$

where t_1 is the closure time for S_1, C = capacitance, and V_o = initial charge voltage. The longitudinal force F on the armature is given as

$$F = \sum_{k=1}^{N_s} \sum_{j=1}^{N_p} I_k I_j \frac{d}{dx} M_{kj} \qquad (7)$$

where x = displacement distance coordinate.

The method for calculating inductance [9], forces, and fields [10] is to numerically evaluate path length integrals. The Neumann formula is evaluated for self and mutual inductances and requires specification of current paths. In some cases the zone or current element cross section is relatively large and multiple paths are required [11]. The self inductances of coil and armature zones are fixed throughout the problem as are the mutual inductances between coils and between

armature circuits. The mutual inductance between coil and armature circuits depends upon armature position, but assuming only longitudinal projectile motion, can be pre-calculated and loaded into a table for interpolation during the simulation. The net longitudinal force on the armature is determined from mutual inductance gradients and derived from this table. If it is desired to compute a force distribution or magnetic fields, then the formulas given in Ref. 10 are applied after the simulation has finished by post-processing output.

Often there is concern that the zone size chosen does not adequately resolve current penetration or skin effects. To account for this in an approximate way, we solve a 1-D diffusion model within each zone at each time step and compute an effective skin depth. This is done by subdividing the zone, treating the penetration as one dimensional, and forcing the total zone current to equal the value given by the circuit model. An internal symmetry boundary condition is also assumed. Given the internal current density distribution, the effective skin depth is computed and the zone resistance modified. In most cases this is a small correction. If it becomes a large correction, re-zoning of the problem is required. A similar approach is used to make skin resistance corrections to coil circuits. For coil circuits the magnetic field is assumed as the dependent variable and a 1-D diffusion equation solved in the radial direction. Here zero field is assumed on the outside of the coil and the appropriate B field jump condition across each coil layer. Again, the current density is determined and the skin resistance correction computed for the coil. In addition to the radial distribution of current within the windings, there is a longitudinal bunching. The effect of this proximity is modeled following the work of Welsby [8] and results in a further increase in coil resistance.

An example of an armature and coil is shown in Fig. 2. Note the armature is subdivided into non-uniform zones and the coil is a single layer, 8-turn coil for this example. The armature is shown in the centered position. In the multi-stage launcher the coils are located close to one another with a spacing of only .02 m for the example shown. The launch payload mass is treated as an external point mass that is added to the armature mass when computing acceleration. Initially, the rear edge of the armature is positioned inside the coil and there is a magnetic gradient and longitudinal force at the rear of the projectile. As time advances, the magnetic field diffuses forward in the armature and

the firing position of a given stage is advanced forward with respect to the armature. This induces a traveling wave in the armature with a slip velocity given by the rate at which the firing position is advanced. If the wavelength is held fixed by selection of stage capacitance and coil inductance, then a traveling wave can be reasonably approximated.

Figure 2. Coil and armature configuration showing circuit geometry for a single centered coil stage. Multistage problems have many additional stages separated by a small longitudinal space. The configuration is that of the point design calculation given below.

CALCULATION

A point design has been completed for a full scale ETO launcher using WARP-10. Final velocity was to be greater than 4 km/s for a 450 kg armature and a 400 kg flight mass. Acceleration was to be < 1.5 kgees. Other variations on this point design appear possible as does further optimization.

Set-up parameters of the point design are the following: armature mass 450 kg, non-armature mass 400 kg, armature material 7075-T73 Al, armature o.d. = .496m, armature i.d. = 0.328 m, length = 1.49 m, and initial temperature = -196 deg C. The coil i.d. = .54 m, coil length = .18 m, coil material = Al, 8 turns, coil inductance change/final inductance = .54 assuming a perfectly conducting projectile, and coil inductance = 44.5 microhenry with no projectile. Stage separation (center-to-center) = .2 m, number of stages = 3100, launcher length = 620 m, crowbar when diode voltage = 0, stored energy/stage = 5 MJ, maximum voltage = 182 kV, peak coil current = 395 kA, pulse quarter wave length = .4 m, and slip velocity = 2 m/s.

Results of the calculation are shown in Fig. 3. This figure shows the acceleration history for the first 240 stages. Note that in about 100 stages the acceleration rises to a steady state value of 1.4 kgees with a superimposed fluctuation of ± 7%. This fluctuation level results because the coils have some longitudinal extent and small reverse currents can build in the armature surface between stages. These fluctuations can be reduced with shorter coils if so desired; there is no significant effect on armature heating or performance from these fluctuations for the problem considered, however.

Figure 3. Launch mass acceleration vs time for stages 1 - 240 of the ETO point design.

Figure 4. Coil current vs time for ETO stages 1 - 240.

Figure 4 shows that coil currents overlap in time and consequently a force is exerted on the armature from several coils at any given time. The current traces are truncated in the plot. We typically find that the peak coil current does not occur at zero capacitor voltage but is influenced by the large inductance change in the coil circuit as the projectile moves forward. Although not shown, the coil currents decay rapidly following the diode turn-on as a dump resistor is added to the circuit. A further increase of system efficiency is possible by letting the coil energy ring back into the capacitor with recovery for the next shot. This energy recovery was not considered here because of concerns of reduced capacitor lifetime from reversed voltage.

The circulating current in the armature is shown in Fig. 5 and is seen to have a large "dc" component with superimposed fluctuations. The mechanism for this is as described above. The fluctuation period t_f decreases with velocity and is about equal to the stage transit time, i.e. $t_f = d_s/v$, where d_s = stage length and v = armature velocity.

For higher velocities, the acceleration is seen in Fig. 6 to be at a nearly constant level with superimposed fluctuations. The average acceleration is found to be about 1.42 kgees with a peak/average ratio of 1.05.

Figure 5. Circulating current components in the armature.

Figure 6. Acceleration vs time for ETO stages 2861 to 3100.

For this point design we obtained a final velocity of 4149 m/s and an efficiency of 47.2 % (kinetic energy/stored energy). Ohmic heating in the armature was quite small with a maximum temperature of only 19°C (locally) and a final ohmic energy/kinetic energy ratio of 0.00146.

We could have continued the calculation to higher velocity, as we are far from being limited by heating at this velocity. Alternatively, only about 2/3 of the armature was exposed to magnetic fields and currents. We could have used a 300 kg armature with a 550 kg launch payload with the same armature heating and

performance if we had so chosen. This was not calculated, however.

The entire calculation was performed on a CRAY computer and required about 15 separate runs and about 20 hours of CPU time. This calculation demonstrated the feasibility of a full scale ETO induction launcher and showed the practicality of performing system design using the WARP-10 code. This point design is by no means optimum, and alternative sizes and different armature-payload combinations are under study. Based upon the point design calculation, we expect further improvements in performance and tolerable armature heating for a wide variety of launcher parameters.

DISCUSSION

As was mentioned above, the mode of operation is that of a traveling wave induction launcher following an initial phase of establishing the induced current in the armature. The coils are actively synchronized with the armature and the slip provided by advancing the fire position. There are differences from the usual traveling wave accelerator. First, the wave extends in one direction from the fire position and operates initially on the rear of the projectile. There are no end effects on the front of the armature that could lead to retarding forces. Also, the payload structure that would be located to the front of the armature is not exposed to traveling waves sweeping across the armature. The armature in this case is solid metal and can be comparable in thickness to the current penetration depth. Finally, the armature thickness allows support of the radial forces on the armature that lead to significant hoop stress. Thin armatures or wound armatures would have greater difficulty in supporting these stresses.

Earlier work by Elliot [12] has predicted performance of traveling wave launchers in which he predicted the armature heating was directly dependent on the slip velocity v_s and projectile velocity v as

$$\text{Ohmic Power/Kinetic Power} = v_s/v \qquad (8)$$

We essentially confirm this dependence, although the agreement is not exact since we are only approximating a traveling wave system. Also, the early portion of the launch during which the wave is being established has heating at reduced performance, thereby increasing the ohmic/kinetic energy ratio.

Scaling simulation calculations are in progress from which we find improved performance for a reduced armature resistivity. Also, there is an optimum slip velocity for performance. Efficiencies as high as 60 % have been calculated in short runs with only a few hundred stages. These results will be the subject of a future report. Further reductions in the acceleration fluctuations have also been achieved in more recent calculations (not shown) where the peak/average acceleration is less than 1.01.

Separate calculations (not shown) also predict that slip velocity can be reduced as size is increased for the same high efficiency. Consequently, ohmic heating is reduced (Eq. 8) and a higher velocity is possible as size is increased.

CONCLUSIONS

A numerical simulation model is outlined here that can predict from first principles the performance and armature heating for operation of a contactless coil launcher. WARP-10 has been applied to the ETO application and predicts that basic operation of such a launcher is technically feasible. Operation of the launcher is understood from scaling relations appropriate for traveling wave induction launchers, although the excitation method and the field configuration are different from those of other coil launchers [12-15] and are realizable using pulsed capacitor technology and an actively controlled firing system. Calculations predict that high efficiency and very low armature heating are possible with this launcher. Consequently, high velocity should be possible provided the size is sufficiently large. This is the case for the ETO launcher.

ACKNOWLEDGEMENT

This work was supported by the U.S. Department of Energy under contract No. DE-AC04-76DP00789. The author would like to acknowledge helpful discussions with M. Cowan and support for the work from J. P. VanDevender.

REFERENCES

[1] M. Cowan, M. M. Widner, E. C. Cnare, B. W. Duggin, R. J. Kaye, and J. R. Freeman, "Exploratory Development of the Reconnection Launcher, 1986-1989," this meeting.

[2] M. Cowan, E. C. Cnare, W. K. Tucker, and D. R. Wesenberg, "Multimegajoule Pulsed Power Generation

From a Reusable Compressed Magnetic Field Device," International Conference on Energy Storage, Compression, and Switching, Asti-Torino, Italy, November, 1974, Plenum Press, New York, p 131.

[3] T. J. Burgess, E. C. Cnare, W. L. Oberkampf, S. G. Beard, and M. Cowan, "The Electromagnetic Theta Gun and Tubular Projectiles," IEEE Trans. Magn., MAG-18, 46 (1982).

[4] M. Cowan, E. C. Cnare, B. W. Duggin, R. J. Kaye, and T. J. Tucker, "The Reconnection Gun," IEEE Trans. Magn., MAG-22, 1429 (1986).

[5] D. G. Elliott, "Mesh-Matrix Analysis Method for Electromagnetic Launchers," IEEE Trans. Magn., 25, 164 (1989).

[6] E. C. Cnare and M. M. Widner, "A 10-Stage Reconnection Demonstration Launcher," this meeting.

[7] R. J. Kaye, E. L. Brawley, B. W. Duggin, E. C. Cnare, and M. M. Widner, "Design and Performance of a Multistage Cylindrical Reconnection Launcher," this meeting.

[8] V. G. Welsby, The Theory and Design of Inductance Coils, Second Edition, MacDonald, London (1960), Chapter 3.

[9] R. Plonsey and R. E. Collin, Principles and Applications of Electromagnetic Fields, McGraw-Hill, New York (1961), p 275.

[10] P. Hammond, Applied Electromagnetism, Pergamon Press, New York (1985), p 189.

[11] F. W. Grover, Inductance Calculations, Dover Publications, Inc., New York (1973).

[12] D. G. Elliott, "Traveling-Wave Induction Launchers," IEEE Trans. Magn., 25, 159 (1989).

[13] P. Mongeau and F. Williams, "Arc-Commutated Launcher," IEEE Trans. Magn., MAG-18, 42 (1982).

[14] M. D. Driga, W. F. Weldon, and H. H. Woodson, "Electromagnetic Induction Launchers," IEEE Trans. Magn., MAG-22, 1453 (1986).

[15] Z. Zabar, Y. Naot, L. Birenbaum, E. Levi, and P. N. Joshi, "Design and Power Conditioning for the Coil-Gun," IEEE Trans. Magn., 25, 627 (1989).

Figure 1.

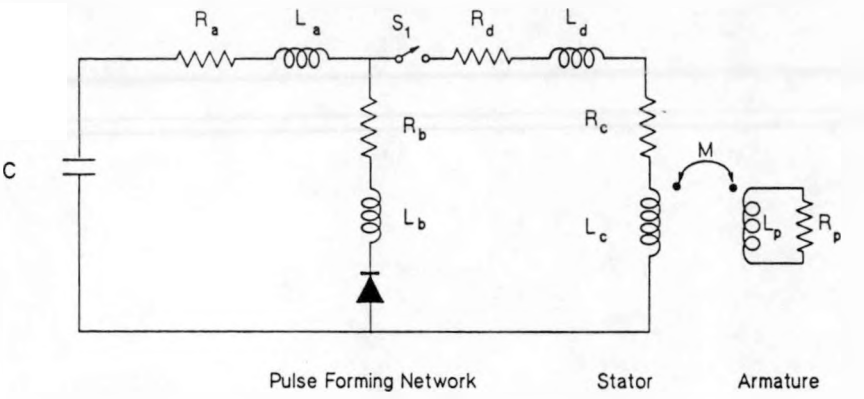

Figure 2.

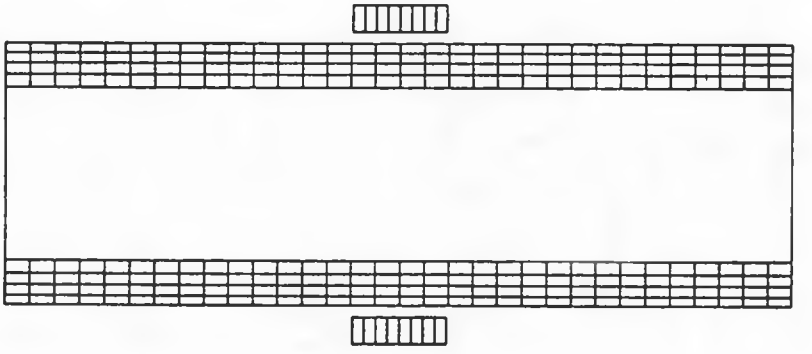

Figure 3.

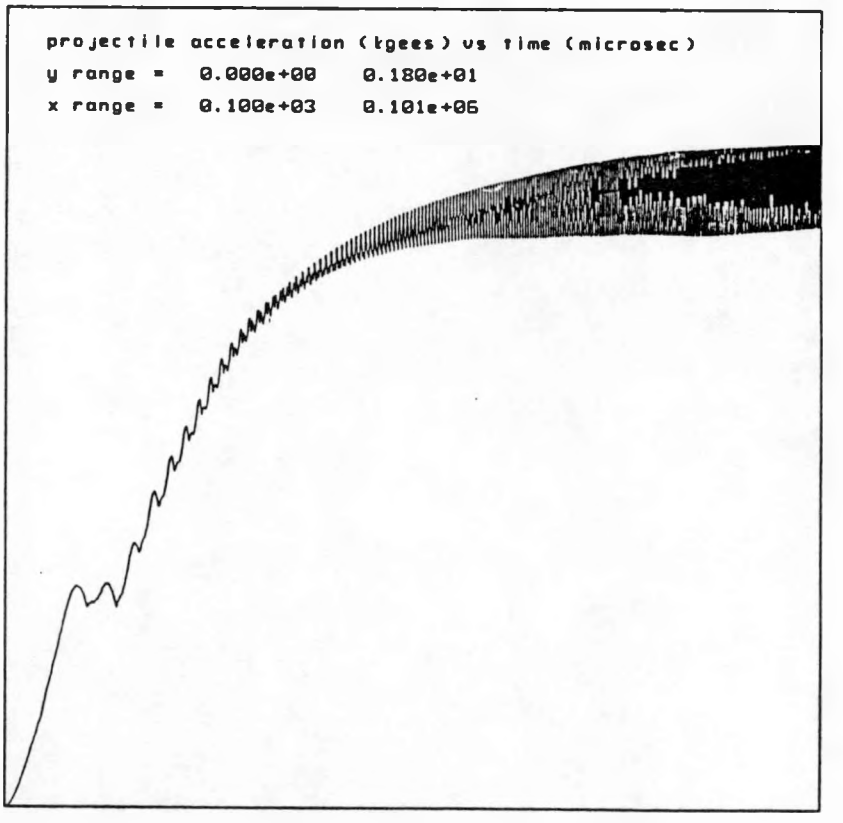

Figure 4.

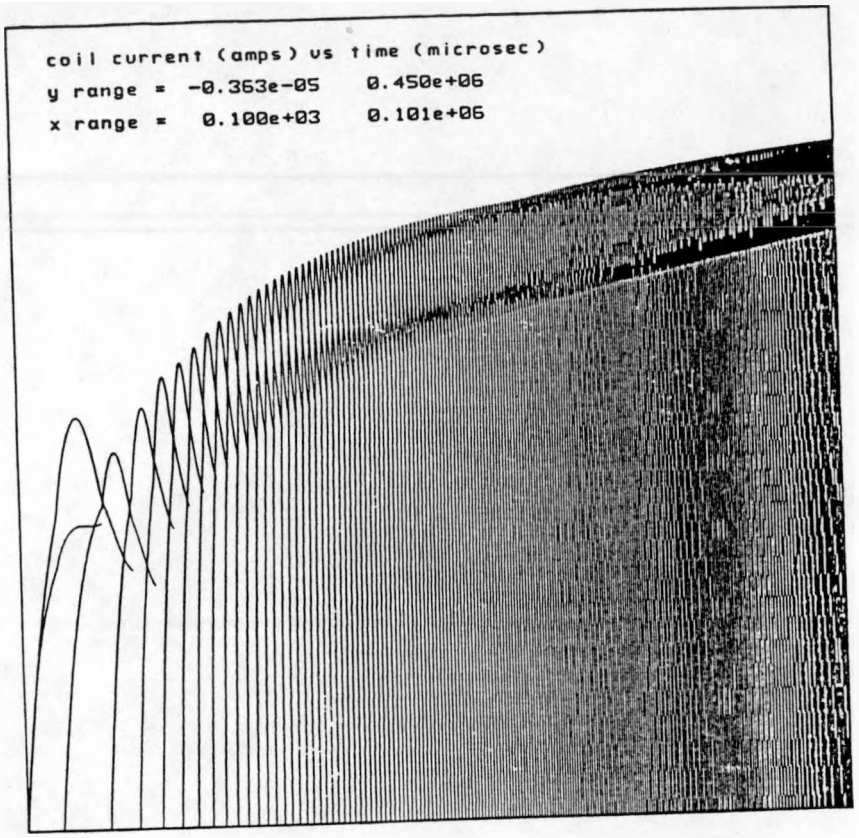

Figure 5.

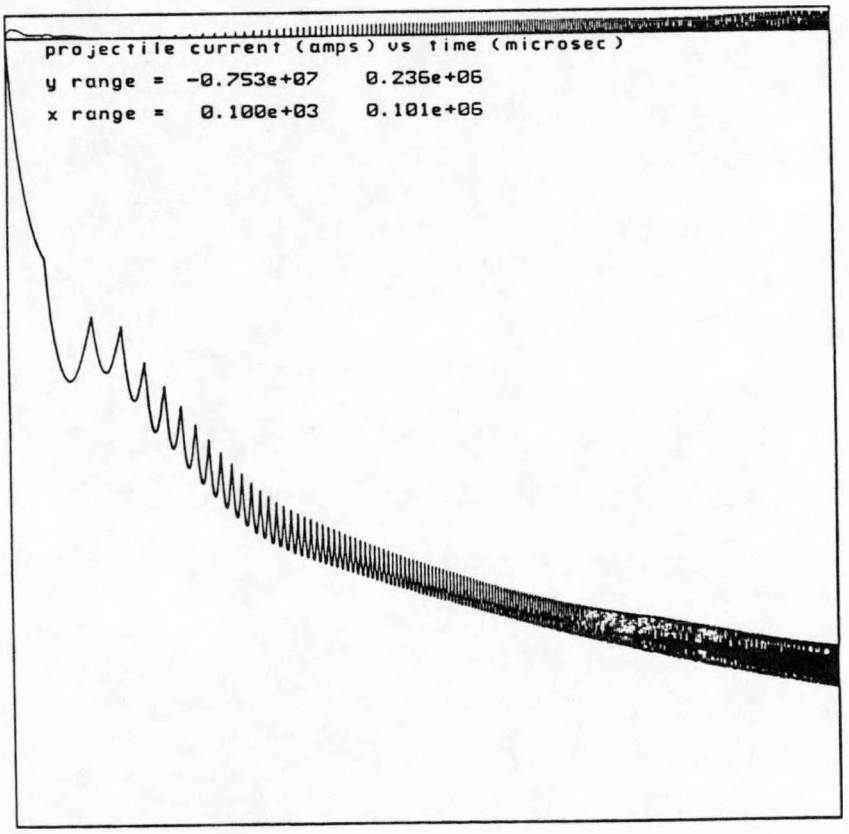

Figure 6.

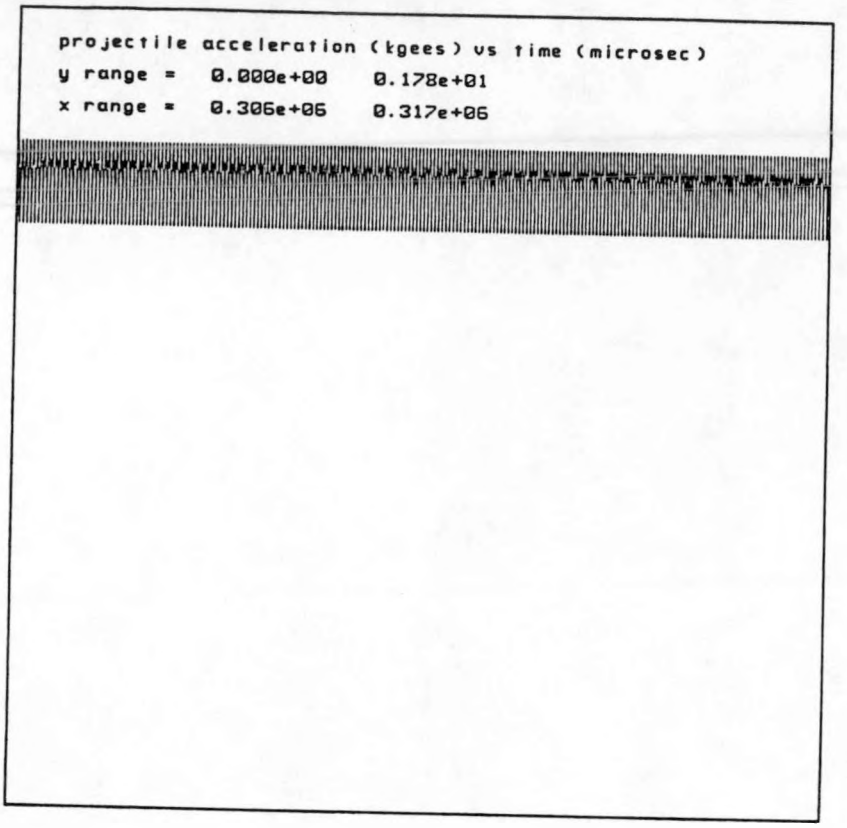
projectile acceleration (kgees) vs time (microsec)
y range = 0.000e+00 0.178e+01
x range = 0.306e+06 0.317e+06